A study of the optical properties of nickel-pigmented anodic alumina in the infrared region

1996 J. Phys.: Condens. Matter 8 5125

(http://iopscience.iop.org/0953-8984/8/27/021)

J. Phys.: Condens. Matter **8** (1996) 5125–5138. Printed in the UK

A study of the optical properties of nickel-pigmented anodic alumina in the infrared region

Ewa Wäckelgård

Solid State Physics, Department of Technology, Box 534, Uppsala University, S-751 21, Uppsala, Sweden

Received 10 January 1995, in final form 18 April 1996

Abstract. The reflectance of nickel-pigmented anodized thin alumina films on aluminium has been measured in the infrared range between 5 and 20 μm. The strong absorption of plain porous alumina, found at around 10 μm for p-polarized light at an oblique angle of incidence and originating from the longitudinal optical phonons interacting with light, is reduced for pigmented alumina. Electrochemical deposition of nickel in the pores of anodic alumina starts from the bottom of the pores, forming a nickel-pigmented bottom layer as the time of pigmentation increases. It is shown from p-polarized reflectance measurements at an oblique angle of incidence that with increasing thickness of the nickel-filled bottom layer the LO mode absorption is decreasing. This is consistent with effective-medium calculations which have been performed using the Maxwell Garnett model. It is found to be an effect of the geometrical shape and orientation of the nickel particles, which for these samples appear as rods with their long axes perpendicular to the sample surface.

1. Introduction

Alumina is used in a variety of technical applications, one of which is as the matrix for small metallic particles in solar absorbers. With the appropriate concentration of metallic particles and the correct film thickness, this cermet layer has good solar selective properties [1–4]. Studies of the solar selective properties of nickel-pigmented anodized aluminium have led to this study of the more fundamental infrared optical properties of cermets reported here. The purpose was to minimize the thermal emittance of the absorber surface.

Commercial solar absorbers of nickel-pigmented aluminium oxide are produced by anodization in phosphoric acid followed by electrochemical deposition of nickel particles in the pores of the alumina. It has been found that anodic alumina formed in phosphoric acid has a larger pore fraction than alumina prepared in other acids [10, 21]. The diameter of the pores can be as large as 200 nm and constitute up to 40% of the total volume [5]. Such a large volume fraction of metal is suitable for obtaining high solar absorption within a film which is more or less infrared transparent since it is much thinner than the infrared wavelengths.

In plain alumina the porosity influences the optical properties. It has been shown that the reflectance minimum at the wavelengths of the longitudinal optical phonon mode observed for p-polarized light at oblique angles of incidence is shifted in wavelength compared to that of non-porous alumina [6]. Optical properties of anodic pigmented alumina in the wavelength range 5–20 μm were not found in a literature survey made for this study. Similar systems of coevaporated Co–Al_2O_3 cermets have been studied in detail in this

0953-8984/96/275125+14$19.50

wavelength range [3]. The dielectric function for cermets containing different filling factors of cobalt was determined from reflectance and transmittance measurements. It was found that metal particles in concentrations below the percolation threshold give rise to a dielectric, non-metallic response to the electric field. The imaginary part of the dielectric function has the same features as that of pure evaporated alumina [7], but the peaks corresponding to the transverse optical phonon modes of alumina are enhanced, just as if the modes have become stronger due to the presence of the metal particles. The real part displays a behaviour that is not currently understood. The real part of the dielectric function of ionic materials is negative between the wavelengths of the transverse and longitudinal optical phonon modes, at least for the LO–TO pair of shortest wavelengths. According to mean-field theory, there should be larger negative values in this range when cobalt particles are present in the alumina [3] but the experimental findings reveal that there is no region with negative values. The experimental values in the vicinity of the longitudinal optical mode are far outside the Bergman–Milton boundaries [8] that describe the theoretical limits of the dielectric function for a two-component composite treated as an effectively homogeneous medium.

In this report, the infrared properties in the wavelength range 5–20 μm are investigated for anodic alumina with nickel-filled pores.

2. Sample preparation

Rolled electroplated aluminium was used as the substrate. The aluminium samples were anodized in 2.5 M phosphoric acid at a constant dc voltage of 15 V for 15 minutes at a temperature of 19.0 ± 0.5 °C. Then pigmentation followed in a solution of 20 g $NiSO_4$, 20 g $MgSO_4$, 20 g $(NH_4)_2SO_4$ and 20 g H_3BO_3 at 15 V ac at room temperature. The ammonium sulphate improves the conductivity of the solution, and magnesium sulphate has been found to improve the colouring conditions [9]. The solution is buffered with boric acid to maintain a pH of about 6.5–7. Two sets of samples were prepared, one for comparisons of the infrared optical properties between plain and pigmented aluminium oxide (samples 1 and 2), and the other, consisting of five samples (samples 3–7), were pigmented for different times and were used to study the gradual change of the reflectance with increased nickel content in the oxide. The samples are presented in table 1.

3. Sample characterization

The oxide film thickness and surface roughness were measured with an Alpha-Step 200 mechanical stylus profilometer. The film thickness was found to be 0.50 ± 0.02 μm with an average roughness of 0.02 μm.

The nickel particles could be seen with SEM by dissolving the oxide in chromic phosphoric acid [10]; they had the appearance of solid rods about 30 nm thick and 0.3 μm long on average for sample 2. There is probably a size distribution, but this was difficult to determine from the SEM images. It has been shown earlier that particles formed electrochemically from nickel sulphates in anodic porous aluminium oxide have a shape which appears to be a cast of the pore which they are formed in [11]. It is also clear from that study that the particles are solid and non-porous. There has been some discussion in the literature about the chemical composition of these particles, but the most rigorous investigation, done by electron diffraction, shows that the particles are metallic [12].

Depth profile measurements have been carried out by using GDOES (glow discharge optical emission spectroscopy). According to these measurements, the pigmented alumina

Table 1. The nickel content of the samples as determined by GDOES. The samples have been anodized identically but pigmented with nickel for different times.

Sample	Pigmentation time (min)	Nickel content (g m^{-2})
1	0	0
2	2	0.83
3	1	0.34
4	2	0.63
5	3	0.79
6	4	0.90
7	5	1.08

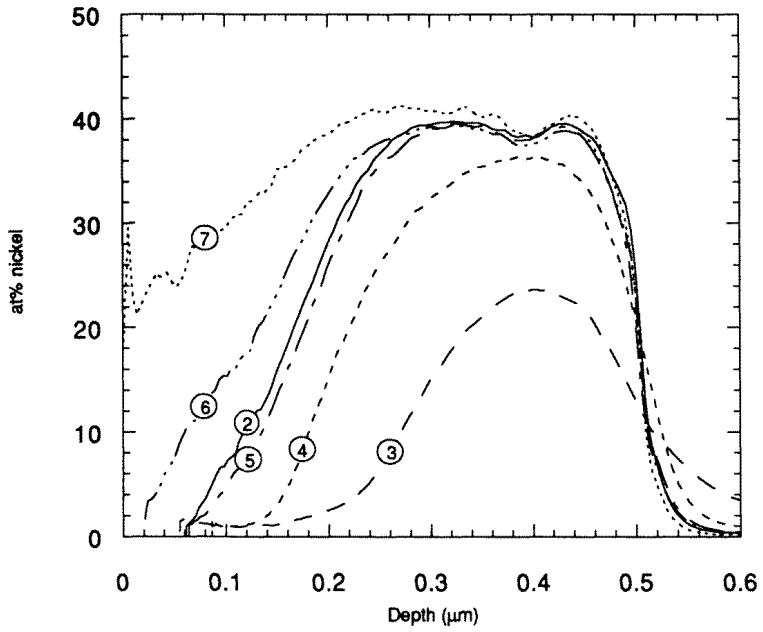

Figure 1. GDOES depth profile measurements showing the nickel content in nickel-pigmented alumina. The sample numbers refer to table 1.

film consists of aluminium, oxygen and nickel. Very small amounts of phosphor contamination from the anodizing electrolytes were also recorded, but there were no detectable remainders of sulphur, magnesium or nitrogen originating from the pigmentation. Figure 1 presents the depth profiles of nickel, and the total nickel content of each sample is tabulated in table 1. The pigmentation starts from the bottom of the pores and they are gradually filled during the course of pigmentation, so the pigmented part of the film increases in thickness and nickel content. From GDOES measurements it is hard to find an average particle size and size distribution since the tail of the nickel content recorded towards the surface is convoluted with an unknown instrumental uncertainty. For this reason, the layer is characterized by a double layer consisting of a bottom layer with nickel in the pores and

a top layer with air-filled pores. A pore fraction of 0.3 is found from TEM pictures on plain porous alumina [6]. Owing to the anisotropic character of the layer, optical anisotropy can be expected.

4. Optical measurements

Spectral specular reflectance was measured in the wavelength range 2–50 μm with a Perkin–Elmer 983 Infrared Spectrophotometer. The reflectance of s- and p-polarized light was measured between 15° and 75° in steps of 5° for sample 2 (table 1) using an accessory for variable angles of incidence. An aluminium film evaporated onto glass was used as a reference. The reflectance data of the samples were divided by the reference spectrum and multiplied by the calculated reflectance of aluminium using optical constants from the literature [13].

For samples 3–7 the reflectance was measured in the wavelength range 5–30 μm for p-polarized light at 75°.

5. Experimental results from optical measurements

Reflectance spectra are presented for s- and p-polarized light for sample 2 in figure 2. The anisotropy of the microstructure with columnar nickel rods perpendicular to the surface is manifested in the large difference in reflectance for s- and p-polarized light at high angles of incidence in the interval 2–4 μm. The broad absorption band for p-polarized light at around 10 μm is due to the longitudinal optical phonon mode of alumina [6].

In figure 3, the effect of nickel content is demonstrated in the p-polarized reflectance at oblique incidence (75°) for samples 1–7. As the amount of nickel increases, the absorption at the LO wavelengths decreases. These changes in the optical properties induced by the presence of the metal particles are discussed later in this paper.

6. Determining the optical constants

Optical constants can be derived solely from reflectance measurements. The method described in [6] has been used here, in which optical constants have been determined by using the Newton–Raphson [14] iterative method to fit the experimental reflectance for p-polarized light measured at 50° and 75° with the Fresnel formulae. It was possible to fit the data in the interval 5–20 μm where the reflectance is significantly different for these two angles of incidence. These optical constants can be interpreted as effective isotropic optical constants, but as they are derived from high-angle p-polarized reflectance, they should mostly resemble the component of the proper anisotropic optical constants perpendicular to the surface. This was previously found to be the case for plain alumina [6]. The validity of treating the cermet as an isotropic medium in the infrared region is shown by the plots in figure 4. The reflectance was calculated for the rest of the angles of incidence measured using the optical constants derived and the Fresnel formulae for an isotropic film on aluminium. The results are shown in figure 4 for three selected angles. The discrepancies between the calculations and the experimental values are quite small. This is also the case for the s-polarized light for which the optical constants fit the data reasonably well. The reason that the anisotropy has such a small influence in this wavelength range is discussed later.

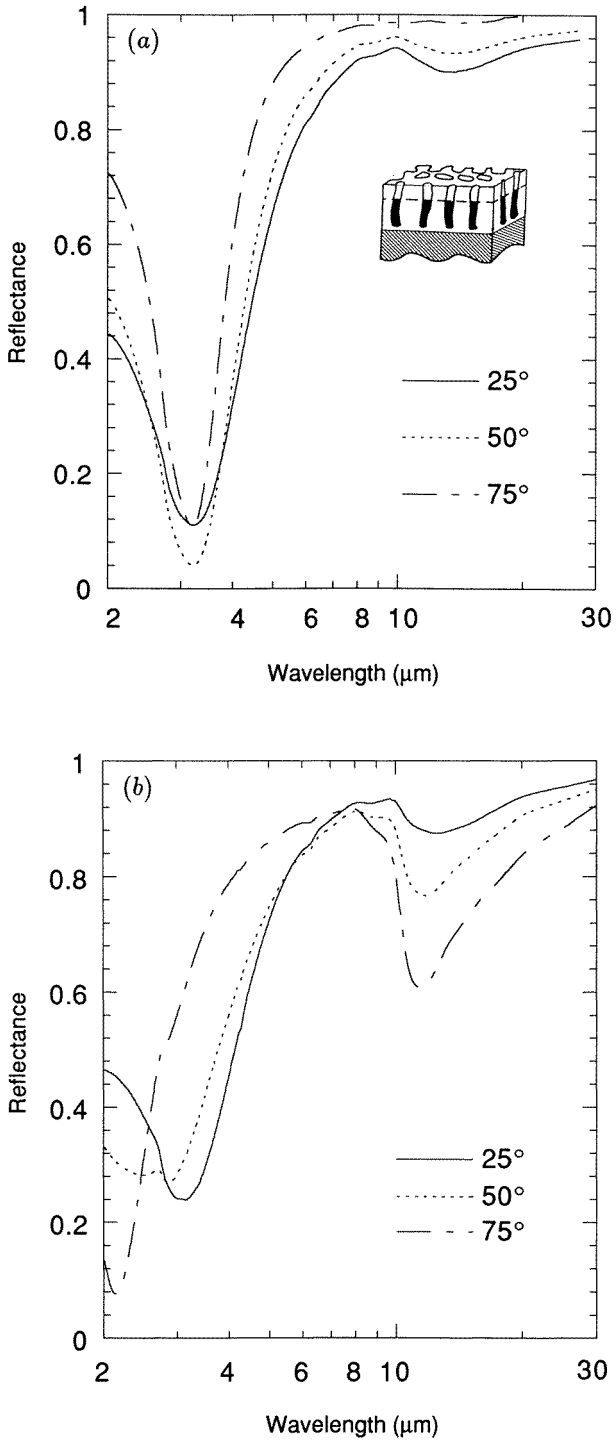

Figure 2. The specular s- (*a*) and p- (*b*) polarized reflectance of nickel-pigmented alumina, sample 2, for three different angles of incidence. The film causes interference pattern in the near-infrared wavelength range.

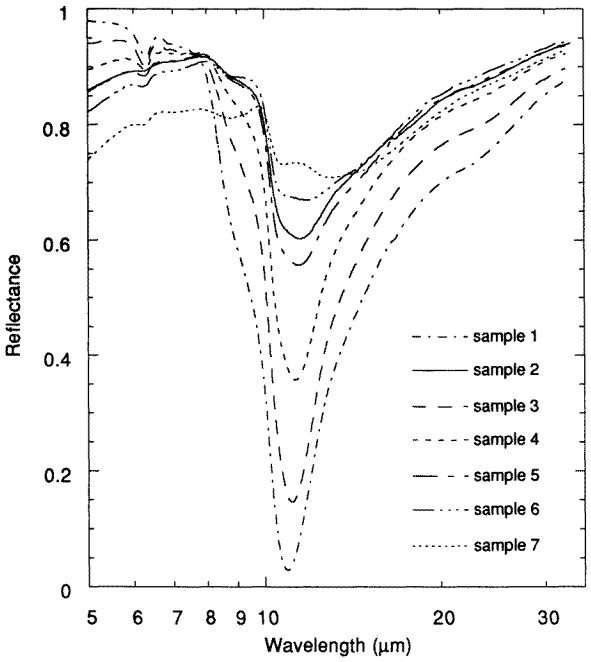

Figure 3. The specular p-polarized reflectance of the nickel-pigmented samples. The sample numbers are the same as in table 1. The angle of incidence of the light is 75°.

7. Theory

The dielectric function calculated from the experimental complex refractive index is presented in figure 5. Error bars are drawn for some experimental points to show the level of uncertainty in different intervals. These were obtained for each point from the combination of $R_{exp} \pm 0.01$, $\theta \pm 0.5$ and the thickness uncertainty of ± 0.02 μm, which gave the largest deviation in the refractive index. For comparison, the experimental dielectric function for the same oxide without nickel, derived with the same method [6], has also been plotted. Both the real and imaginary parts of the dielectric function are enhanced in comparison to the plain porous oxide in the same manner as for evaporated Co–Al_2O_3. The real part is also shifted to higher positive values. The energy-loss function has diminished, which shows that LO absorption has been quenched by the metal particles.

Mean-field theory can be used since the size of the pores in the alumina is smaller than the infrared wavelengths. The same procedure has been followed as for plain porous alumina [6]. Both the Maxwell Garnett and Bruggeman effective-medium models for small particles [15–17] have been used to calculate the dielectric function of the cermet. The results were the same for the two models and therefore only the Maxwell Garnett effective dielectric function is presented here. The shape of the pores is simplified by assuming that they are long cylinders perpendicular to the surface. The dielectric function was calculated for the electromagnetic field perpendicular, ε_z, and parallel, ε_x, to the surface of the sample. The chosen z-coordinate axis also coincides with the long axis of the cylindrical particles. The dielectric function of the electron-beam-evaporated aluminium oxide [7] was used for the dielectric and bulk nickel data [18, 19] for the nickel particles. The equations for the

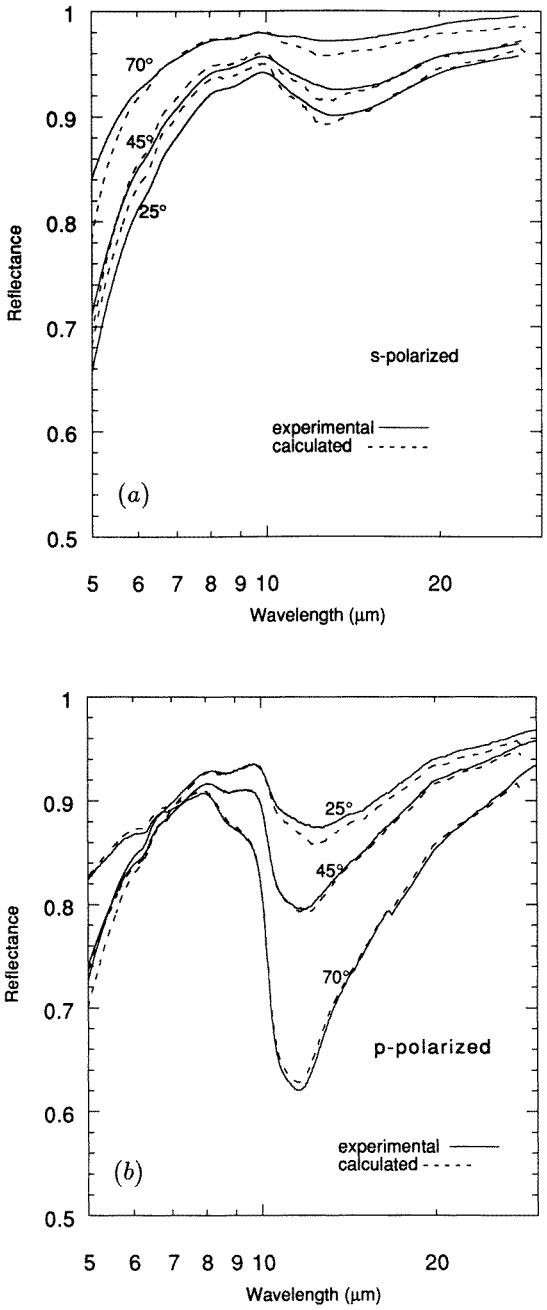

Figure 4. The specular s- (*a*) and p- (*b*) polarized reflectance, experimental and calculated using the optical constants from the fit of Fresnel's formula to the experimental reflectance for 50° and 75° angles of incidence.

Maxwell Garnett effective dielectric function, with the appropriate numerical values for the depolarization (zero in the z-direction and 0.5 in the x-direction) and with a filling factor

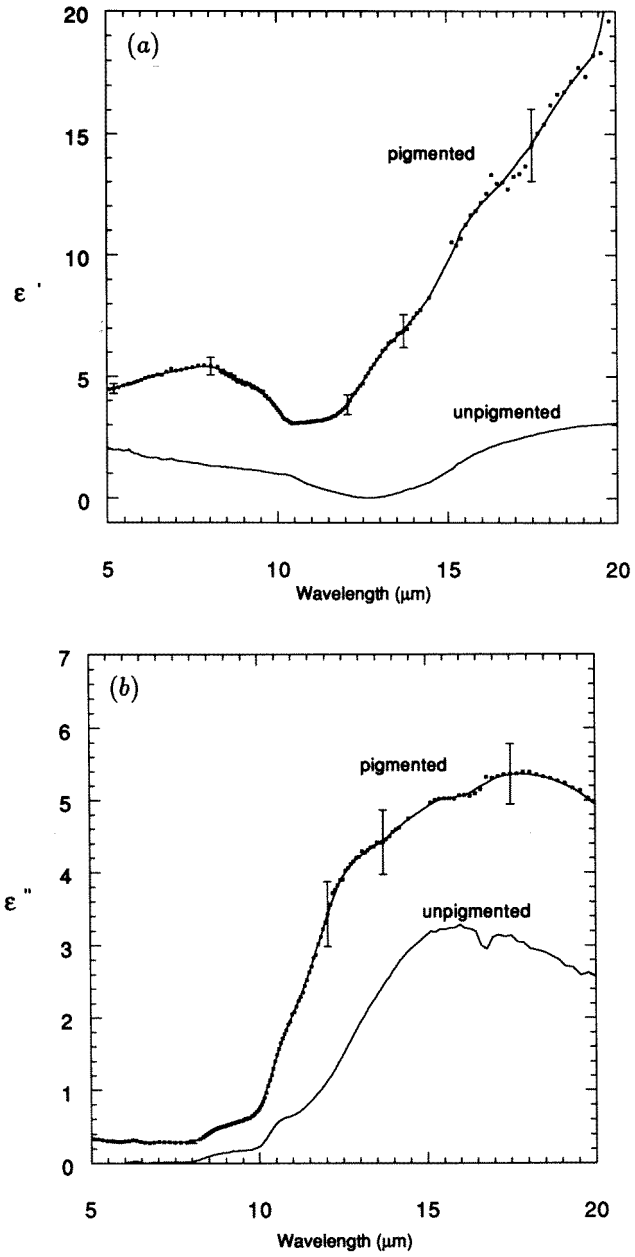

Figure 5. The dielectric function of nickel-pigmented alumina: (*a*) the real part; (*b*) the imaginary part; and (*c*) the energy-loss function. A line fit is shown as a guide to the eye. For comparison the dielectric function of unpigmented alumina, sample 1 [6], is also presented in the figure.

of 0.3 for air in the pores within the top layer ($\varepsilon_{\text{air}} = 1$) are:

$$\varepsilon(\text{alox})_z = 0.3 + 0.7\varepsilon_{\text{oxide}} \tag{1a}$$

$$\varepsilon(\text{alox})_x = \varepsilon_{\text{oxide}}(0.65 + 0.35\varepsilon_{\text{oxide}})/(0.35 + 0.65\varepsilon_{\text{oxide}}) \tag{1b}$$

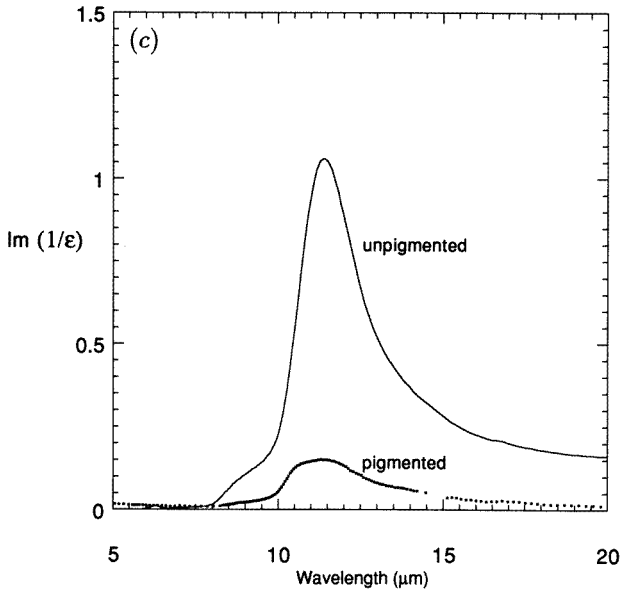

Figure 5. (Continued)

and for the nickel-filled bottom layer with the same filling factor and depolarization factors

$$\varepsilon(\text{nialox})_z = 0.3\varepsilon_{\text{nickel}} + 0.7\varepsilon_{\text{oxide}} \tag{2a}$$

$$\varepsilon(\text{nialox})_x = \varepsilon_{\text{oxide}}(0.65\varepsilon_{\text{nickel}} + 0.35\varepsilon_{\text{oxide}})/(0.35\varepsilon_{\text{nickel}} + 0.65\varepsilon_{\text{oxide}}). \tag{2b}$$

These last two equations show that the anisotropy of the nickel-filled film is large because ε_z is the dielectric function of a metal while ε_x is the dielectric function of a dielectric. The Wiener equations [20] for a stratified structure with total thickness less then the wavelength have been used to calculate the effective dielectric function for the whole layer. For sample 2, the top layer with air-filled pores was determined to be 0.2 μm and the nickel-filled part to be 0.3 μm according to the sample characterization. The Wiener equations then become

$$1/\varepsilon_z = 0.4/\varepsilon(\text{alox})_z + 0.6/\varepsilon(\text{nialox})_z \tag{3a}$$

$$\varepsilon_x = 0.4\varepsilon(\text{alox})_x + 0.6\varepsilon(\text{nialox})_x. \tag{3b}$$

It is clearly seen from these two expressions that both ε_x and ε_z have a dielectric character, and a lower anisotropy is expected, as the calculations shown in figure 6 indicate. The top layer of plain alumina changes the response in the z-direction to a dielectric one. This explains the small anisotropy which was found experimentally. From a comparison of the experimental and calculated dielectric functions in figure 6, it is seen that the theoretical real part is lower than that found experimentally, and vice versa for the imaginary part, but the dielectric function is enhanced in both cases compared to that of plain porous alumina. It can also be noticed that the z-component of the effective dielectric function is closest to the experimental values, which is as expected since the latter are determined from high-angle p-polarized reflectance. A difference of a more fundamental nature is that the real part of the dielectric function has a zero crossing which is not found experimentally. The Wiener bounds [20] were calculated for the wavelengths 5, 11.6 and 17.5 μm and it was found that the experimental effective dielectric function was outside the bounds, except for at the

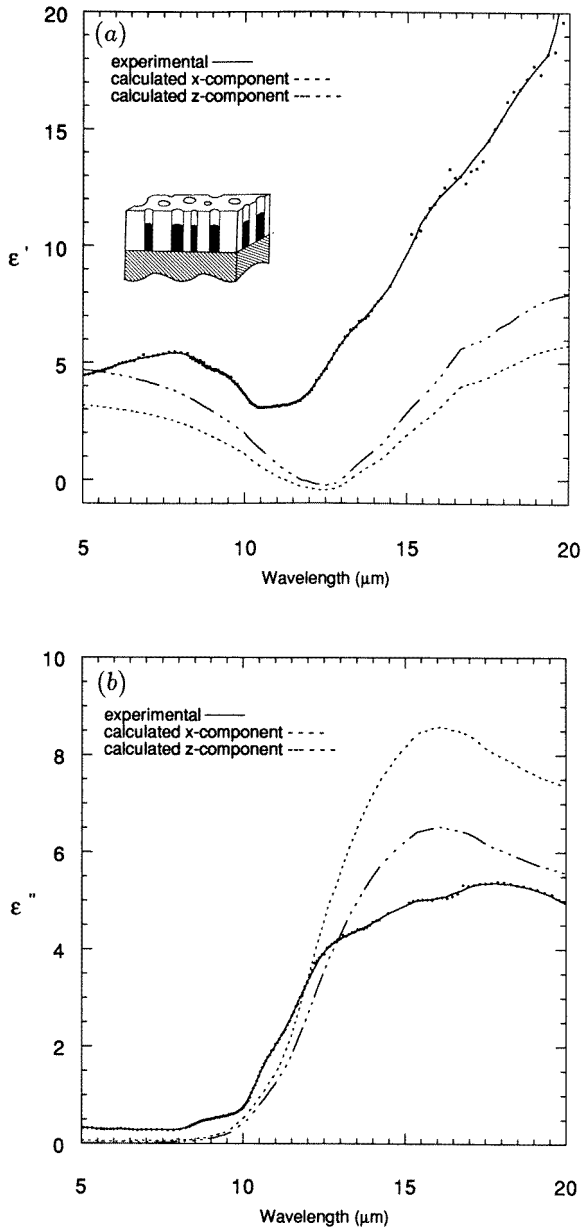

Figure 6. The effective dielectric function obtained using Maxwell Garnett effective-medium theory is compared with the experimental dielectric function of figure 5: (*a*) the real part; (*b*) the imaginary part; and (*c*) the energy-loss function.

shortest wavelength. The Wiener bounds demarcate the region in the complex plane with all possible values of the dielectric function when the filling factor is varied between 0 and 1 using the Wiener equations (equations (3)). The Wiener bounds are used to give a very broad estimate of what can be physically realistic in a two-component composite, which

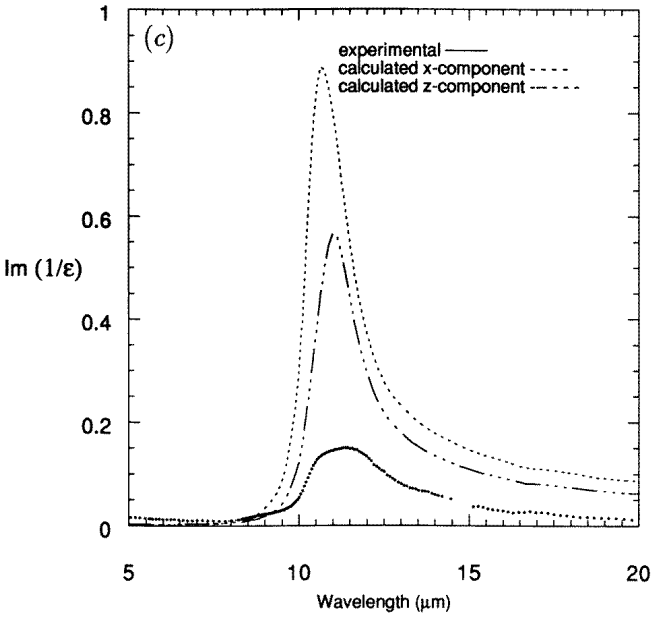

Figure 6. (Continued)

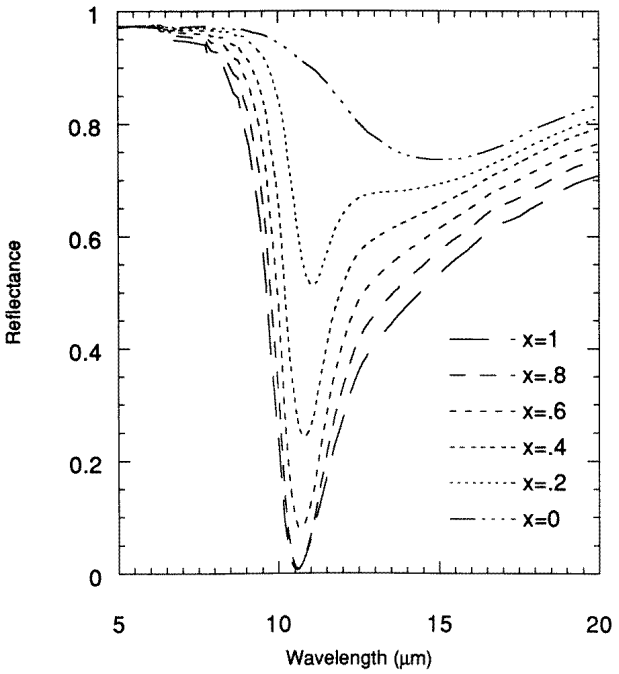

Figure 7. The calculated p-polarized reflectance for a 75° angle of incidence. x symbolizes the ratio of the amount of unpigmented top layer to the total alumina layer of thickness 0.5 μm. The effective dielectric functions of equations (1) and (2) have been used in the calculations.

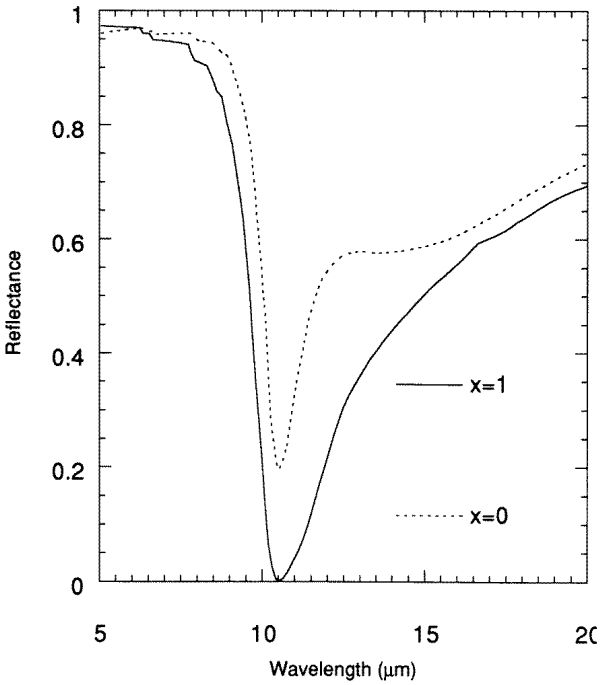

Figure 8. The calculated p-polarized reflectance for a 75° angle of incidence for spherical particles, comparing non-pigmented ($x = 1$) with a fully pigmented ($x = 0$) porous alumina with the same volume fraction 0.3 of nickel/air and film thickness, 0.5 μm, as for the calculations in figure 7.

can be treated as an effective medium in the wavelength range of the measurements. The real part of the dielectric function was far outside the Wiener bounds for the wavelength of the LO mode, 11.6 μm, which means that theory and experiment are in clear contradiction for the interaction between light and LO phonons in cermets. The energy-loss function also reveals this discrepancy between theory and experiment. The theoretical energy-loss function is smaller for the pigmented alumina compared to plain alumina at the LO mode wavelengths, but is not as small as required from an experimental point of view. The z-component of the nickel-pigmented layer is, as mentioned before, the dielectric function of a metal and, because of this, the energy-loss function is close to zero and lacks a maximum. The peak in the energy loss perpendicular to the surface originates from the plain alumina top layer. This is also illustrated by calculations of the p-polarized reflectance at a 75° angle of incidence, presented in figure 7. The reflectance has been calculated for a film 0.5 μm thick, using the effective dielectric function, varying the fractional thickness of the nickel-pigmented layer from 0 to 1 in steps of 0.2. The LO mode absorption is totally quenched when the film is pigmented to the front surface. The theoretical reflectance curves do show the same behaviour as the experimental reflectance (figure 3). The LO absorption is reduced as the pigmented part of the film becomes thicker. Since this is an effect of the geometric form of the nickel particles, for which the z-component of the dielectric function is metallic, the same effect is not expected for spherical particles as is shown in figure 8.

8. Conclusion

The dielectric function for thin nickel-pigmented alumina films on aluminium has been determined in the wavelength range 5–20 μm by fitting high-angle-of-incidence p-polarized reflectance to the Fresnel formula for an isotropic film on aluminium. Rod-like nickel particles in the alumina matrix with their long axis perpendicular to the surface give rise to considerable anisotropy since the character of the dielectric function is metallic for the electromagnetic field perpendicular to the surface and dielectric for fields parallel to it. The anisotropy should be observed experimentally in optical measurements, independently of the wavelength, if the metal particles were to reach the front surface of the alumina film. However, if there is a top layer of plain alumina above the pigmented layer, and both layers have a thickness which is less than the measured wavelength, this large anisotropy vanishes and the dielectric function behaves as a dielectric in both directions. This explains why the isotropic experimental dielectric function can be used to calculate both the s- and p-polarized reflectance as shown in figure 4 in the wavelength range 5–20 μm.

The large difference between the experimental and theoretical values of the real part of the dielectric function in the wavelength range around the LO mode was also seen in coevaporated Co–Al_2O_3 [3]. There is currently no explanation for this. However, the reflectance calculated using the Maxwell Garnett model does reproduce the important features of the reflectance found in the experimental measurements of nickel-pigmented anodic alumina. It is clear from these calculations that the quenching of the LO mode absorption is an effect of the special geometry of the metallic particles. It is this that makes the depolarization factor zero perpendicular to the surface causing a metallic response to the electromagnetic field and no LO mode absorption. The measured reflectance at wavelengths corresponding to the LO mode can be used to estimate the partial thickness of the pigmented layer if the reflectance of unpigmented alumina of the same thickness and prepared under the same conditions is used as a reference.

Acknowledgments

Dr Gunnar Niklasson is acknowledged for good advice and fruitful discussions, research engineer Rein Kalm for assisting with the SEM measurements and Dr Arne Bengtsson for the GDOES measurements.

This work was financed by the Swedish Council for Building Research (BFR) and Marcus and Amalia Wallenberg's Foundation.

References

[1] Blain J, LeBel C, Saint-Jacques R G and Rheault F 1985 *J. Appl. Phys.* **58** 490–4
[2] Uchino H, Aso S, Hozumi S, Tokumasu H and Yoshioka Y 1979 *Natl Tech. Rep.* **25** 994–1004
[3] Niklasson G A and Granqvist C-G 1984 *J. Appl. Opt.* **55** 3382–410
[4] Wäckelgård E, Chibuye T and Karlsson B 1990 *North Sun '90, Solar Energy at High Latitudes (Reading, 1990)* (Oxford: Pergamon) pp 177–82
[5] Nakamura S, Saito M, Huang L-F, Miyagi M and Wada K 1992 *Japan. J. Appl. Phys.* **31** 3589–93
[6] Wäckelgård E 1996 *J. Phys.: Condens. Matter* **8** 4289–99
[7] Eriksson T S, Hjortsberg A, Niklasson G A and Granqvist C G 1981 *Appl. Opt.* **20** 2742–5
[8] Bergman D J 1982 *Ann. Phys., NY* **138** 78
[9] Sheasby P G and Cooke W E 1974 *Trans. Inst. Metall. Finishing* **52** 103–6
[10] Keller F, Hunter M S and Robinson D L 1953 *J. Electrochem. Soc.* **100** 411–9
[11] Pontifex G H, Zhang P, Wang T L, Haslett T L, Al Mawlawi D and Moskovits M 1991 *J. Phys. Chem.* **95** 9989–93

[12] Sandera L 1973 *Aluminium* **49** 533–9
[13] Shiles E, Sasaki T, Inokuti M and Smith D Y 1980 *Phys. Rev.* B **22** 1612
[14] Press W H, Flannery B P, Teukolsky S A and Vetterling W T 1986 *Numerical Recipes, The Art of Scientific Computing* (Cambridge: Cambridge University Press)
[15] Garnett J C M 1904 *Phil. Trans. R. Soc.* **203** 385
[16] Garnett J C M 1906 *Phil. Trans. R. Soc.* **205** 237
[17] Bruggeman D A G 1935 *Ann. Phys., Lpz.* **24** 636
[18] Lenham A P and Treherne D M 1966 *Optical Properties and Electronic Structure of Metals and Alloys* ed F Abéles (Amsterdam: North-Holland)
[19] Siddiqui A S and Treherne D M 1977 *Infrared Phys.* **17** 33
[20] Wiener O 1912 *Abh. Sächs. Akad. Wiss. Lpz. Math.-Naturwiss.* **32** 509
[21] Pavlovic T and Ignatiev A 1986 *Thin Solid Films* **138** 97–109